Relativistic mergers of compact binaries in clusters: the fingerprint of the spin

Patrick Brem,[1][*] Pau Amaro-Seoane[1] and Rainer Spurzem[2,3,4]

[1]*Max Planck Institut für Gravitationsphysik (Albert-Einstein-Institut), D-14476 Potsdam, Germany*

[2]*National Astronomical Observatories of China, Chinese Academy of Sciences, 20A Datun Lu, Chaoyang District, 100012 Beijing, China*

[3]*Astronomisches Rechen-Institut, Mönchhofstraße 12-14, Zentrum für Astronomie, Universität Heidelberg, D-69120 Heidelberg, Germany*

[4]*Kavli Institute for Astronomy and Astrophysics, Peking University, 100871 Beijing, China*

ABSTRACT

Dense stellar systems such as globular clusters and dense nuclear clusters are the breeding ground of sources of gravitational waves for the advanced detectors LIGO and Virgo. The stellar densities reached in these systems lead to the dynamical formation of binaries at a rate superior to what one can expect in regions of the galaxy with lower densities. Hence, these systems deserve a close study to estimate rates and parameter distribution. This is not an easy task, since the evolution of a dense stellar cluster involves the integration of N bodies with high resolution in time and space and including hard binaries and their encounters and, in the case of gravitational waves, one needs to take into account important relativistic corrections. In this work, we present the first implementation of the effect of spin in mergers in a direct-summation code, NBODY6. We employ non-spinning post-Newtonian (PN) corrections to the Newtonian accelerations up to 3.5 PN order as well as the spin–orbit coupling up to next-to-lowest order and the lowest order spin–spin coupling. We integrate spin precession and add a consistent treatment of mergers. We analyse the implementation by running a set of two-body experiments and then we run a set of 500 simulations of a stellar cluster with a velocity dispersion set to a high value to induce relativistic mergers to set a proving ground of the implementation. In spite of the large number of mergers in our tests, the application of the algorithm is robust. We find in particular the formation of a runaway black hole (BH) whose spin decays with the mass it wins, independently of the initial value of the spins of the BHs. We compare the result with 500 Monte Carlo realizations of the scenario and confirm the evolution observed with our direct-summation integrator. More remarkably, the subset of compact objects that does not undergo many mergers, and hence represent a more realistic system, has a correlation between the final absolute spin and the initial choice for the initial distribution, which could provide us with information about the evolution of spins in dense clusters once the first detections have started.

Key words: black hole physics – gravitational waves – galaxies: star clusters: general.

1 INTRODUCTION

The field of gravitational wave (GWs) has reached a milestone in the last years with the build-up of an international network of GW interferometers which have achieved their design sensitivity. The ground-based detectors LIGO and Virgo are undergoing major technical upgrades that will increase the volume of the observable Universe by a factor of a thousand, which is referred to as the 'advanced' configuration.[1]

Dense stellar systems such as globular clusters, galactic nuclei and, in particular, dense nuclear clusters, are the breeding ground of the sources that the advanced detectors can expect (see the recent updated review of Benacquista & Downing 2011 and also Downing et al. 2011). More remarkably, the event rate of stellar-mass black

---

[*] E-mail: Patrick.Brem@aei.mpg.de

[1] http://www.ligo.caltech.edu/advLIGO/, http://wwwcascina.virgo.infn.it/advirgo/

hole binaries, the loudest kind of source, will be likely *dominated by sources formed dynamically*, i.e. via stellar close interactions in these stellar systems (Miller & Lauburg 2009; Banerjee, Baumgardt & Kroupa 2010; Downing et al. 2010; Benacquista & Downing 2011).

The data that will be harvested from the advanced detectors will allow us to do GW astrophysics. The construction of templates for matched filtering is crucial in the searches for compact binaries. There have been efforts to construct these templates by combining post-Newtonian (PN) calculations of the inspiral of the binary with numerical relativity simulations of the merger and ringdown. Two appealing approaches are the effective-one-body technique (Buonanno & Damour 1999; Buonanno et al. 2009) and the phenomenological hybrid waveform modelling (Ajith et al. 2007, 2009; Santamaría et al. 2010).

However, the search will be challenging for the simple reason that a GW has not been detected yet. Reliable estimates of the event rates for the different kinds of binaries and of the expected parameter distribution will possibly be crucial for a successful detection. On the other hand, once we have the data, we will be able to compare the observed rates and parameters with the predictions derived from different models and thus filter them. This will enlighten our understanding of the creation and evolution of compact binaries in dense stellar systems.

The most accurate simulations of dense stellar clusters that we can do nowadays are performed with the so-called direct-summation *N*-body algorithms. In particular, the family of integrators of Sverre Aarseth has been in development for many decades (von Hoerner 1960, 1963; Aarseth 1963). Aarseth's NBODY6 includes both *KS regularization* (where KS stands for Kustaanheimo-Stiefel) and *chain regularization*: when particles are tightly bound or their separation becomes too small, the system is regularized (see Kustaanheimo & Stiefel 1965; Aarseth 2003) to avoid too small individual time steps and numerical errors. It also employs the Ahmad–Cohen neighbour scheme (Ahmad & Cohen 1973) and hierarchical, adaptive time steps. We can hence resolve and follow accurately individual orbits in the system. In this article, we present the first modification of a direct-summation code, using NBODY6, that includes all non-spinning PN corrections up to 3.5PN order and all spin contributions up to 2.5PN order, including spin precession equations.

2 THE FORMALISM AND ITS IMPLEMENTATION

2.1 Correction of the accelerations

We modify the acceleration computation as described in the pioneering work of Kupi, Amaro-Seoane & Spurzem (2006) (KAS06) to include relativistic corrections, which are based on the PN formalism for the interaction between two bodies. We note that recently Aarseth (2012) included an approximative implementation for relativistic corrections in the new version of his code, NBODY7. The relative acceleration, in the centre-of-mass form, including all PN corrections used in the code can be written in the following way:

$$\frac{\mathrm{d}\boldsymbol{v}}{\mathrm{d}t} = -\frac{Gm}{r^2}[(1+A)\boldsymbol{n} + B\boldsymbol{v}] + \boldsymbol{C}_{1.5,\mathrm{SO}} + \boldsymbol{C}_{2,\mathrm{SS}} + \boldsymbol{C}_{2.5,\mathrm{SO}}, \quad (1)$$

where $\boldsymbol{v} = \boldsymbol{v}_1 - \boldsymbol{v}_2$ is the relative velocity vector, $m = m_1 + m_2$ the total mass, r the separation and $\boldsymbol{n} = \boldsymbol{r}/r$. A and B are coefficients that can be found in Blanchet & Iyer (2003). The spin terms $\boldsymbol{C}_{\mathrm{N}}$, where N denotes the PN order, are taken from Faye, Blanchet &

Buonanno (2006) and Tagoshi, Ohashi & Owen (2001). SO stands for spin–orbit and SS for spin–spin coupling.

These corrections are valid for two *isolated* bodies and shall thus only be applied to the Newtonian acceleration in the case of strong, 'relativistic' pair interactions where the perturbation by third bodies is sufficiently small. Because of this, we deem it reasonable to restrict the implementation of PN terms to regularized KS pairs (see Kustaanheimo & Stiefel 1965; Aarseth 2003, for details). For this reason, we also choose the centre-of-mass formulation shown in equation (1) rather than the formulation in the general frame. These KS pairs are only formed when the interaction between two bodies becomes strong enough so that the pair has to be regularized. During the KS regularization the relative motion of the companions is still far from relativistic. Hence, only a small, relativistic subset of all regularized KS pairs will need PN corrections. In order to match the order of accuracy of the KS integration in the code, we compute both the acceleration as shown in equation (1) as well as the analytical time derivative.

To save computational costs, we switch on the PN corrections only if one of the following two conditions is fulfilled:

$$v > \beta c$$

$$v > \frac{\beta}{5}c \quad \text{and} \quad \frac{g_{\mathrm{PN}}}{g} > \gamma_{\mathrm{rel}}, \quad (2)$$

where the parameters β and γ are chosen empirically to be $\beta = 0.02$ and $\gamma = 0.01$ and g_{PN} and g are the PN acceleration and the Newtonian acceleration, respectively.[2] Note that this treatment differs from Aarseth (2012), who chooses a staggered scheme to switch on first PN 2.5, and later PN1 or PN2. We always switch on the complete set if equation (2) is fulfilled in order to maintain a correct orbit integration under PN influence. The switch-on criterion for the PN terms does not depend on the Newtonian perturbation of the regularized pair. Thus, we also apply PN corrections to binaries that are being influenced by a third body. However, we note that for strong perturbations, NBODY6 automatically breaks up the KS pair and uses a Chain regularization algorithm for more than two bodies, in which we do not include any PN treatment due to the complications that arise by having more than two dominant objects.

2.2 Spin precession

In addition to the effects on the acceleration, the spin of compact objects undergoes precession in relativistic two-body interactions. This is also taken into account by integrating the spin precession equations

$$\frac{\mathrm{d}\boldsymbol{S}}{\mathrm{d}t} = \frac{1}{c^2}\boldsymbol{U}_{1,\mathrm{SO}} + \frac{1}{c^3}\boldsymbol{U}_{1.5,\mathrm{SS}} + \frac{1}{c^4}\boldsymbol{U}_{2,\mathrm{SO}}, \quad (3)$$

$$\frac{\mathrm{d}\boldsymbol{\Sigma}}{\mathrm{d}t} = \frac{1}{c^2}\boldsymbol{v}_{1,\mathrm{SO}} + \frac{1}{c^3}\boldsymbol{v}_{1.5,\mathrm{SS}} + \frac{1}{c^4}\boldsymbol{v}_{2,\mathrm{SO}}, \quad (4)$$

$$\boldsymbol{S} = \boldsymbol{S}_1 + \boldsymbol{S}_2, \quad (5)$$

$$\boldsymbol{\Sigma} = m\left(\frac{\boldsymbol{S}_2}{m_2} - \frac{\boldsymbol{S}_1}{m_1}\right). \quad (6)$$

---

[2] In order to avoid confusion, we denote the acceleration with the letter g, the dimensionless spin parameter with a and the semimajor axis with ξ.

S and Σ describe the spin state of the pair. The individual terms for U_N and v_N, where N denotes the PN order, can be found in Faye et al. (2006) and Buonanno, Chen & Vallisneri (2003).

2.3 Relativistic mergers

Since relativistic binaries lose energy via the dissipative 2.5PN acceleration term, we need to consistently add a relativistic 'merger recipe' in the standard version of the code. For the purposes of our study, we must address the following points.

(i) The criterion for two bodies to be transformed into one.

(ii) A dynamically correct treatment of the 'loss' of one object from the simulation.

(iii) Computation of the spin of the BH that is formed after coalescence from the spins and OAM of the BHs that participated in the coalescence.

PN theory can only be applied to the inspiral of the binary, but not to the actual merger and ringdown. We choose for up to 3.5 PN order a cut-off distance of $5 R_S$, with $R_S = 2 G(m_1 + m_2)/c^2$ the combined Schwarzschild radius (Yunes & Berti 2008). For any instantaneous separation below this value, the pair is merged into one body.

On the other hand, the newly formed compact object must have a mass and a velocity vector consistent with the conservation of linear momentum. Also, since we are treating spinning compact objects, all BHs must have an initial spin vector. As we will see ahead, in Section 3, we use a fitting formula at the last integration step before merging the bodies, i.e. at a separation of $5 R_S$, to assign a new spin value to the merged system following the prescription of Rezzolla et al. (2008).

The work we present in this article should be envisaged as a first testing of the algorithm with a 'stress test': Our goal is the integration of a large number of relativistic mergers in a stellar cluster. We achieve this, as we will see later, by setting initially the cluster in a relativistic stage with an extremely large central velocity dispersion. In order to maximize the number of mergers, we neglect the recoil of coalescing pairs, since merging BHs with a very large recoiling velocity could leave the system. However, a priori it is straightforward to implement a recipe for the gravitational recoil by following a similar fitting formula as in, e.g. the work of Pollney et al. (2007); Lousto et al. (2010).

3 TESTING THE IMPLEMENTATION

In this section, we test the implementation itself in a direct-summation code. We present tests with a two-body integrator based on the same routines as NBODY6, but restricted to a simple, regularized two-body system. This is exactly the part of the modification in the integration that we aim at implementing in NBODY6, and hence is a perfect testing ground of our algorithm.

In order to do so, we will compare our simple integrations with theoretical approaches. In this regard, the formulæ of Peters (1964) are useful for testing the orbital decay in the simple non-spinning case. For spinning pairs, we will check the precession frequencies and conservation of the total angular momentum.

3.1 Non-spinning, merging relativistic binaries

In this section, we compare the results of our approximation with the derivation of Peters (1964) of the evolution of the eccentricity and semimajor axis of a binary which is decaying via the emission of GWs. His derivations are based on Keplerian orbits and mimic the 2.5 dissipative term in the PN expansion.

$$\left\langle \frac{d\xi}{dt} \right\rangle = -\frac{64}{5} \frac{G^3 m_1 m_2 (m_1 + m_2)}{c^5 \xi^3 (1 - e^2)^{7/2}} \left(1 + \frac{73}{24} e^2 + \frac{37}{96} e^4 \right)$$

$$\left\langle \frac{de}{dt} \right\rangle = -\frac{304}{15} e \frac{G^3 m_1 m_2 (m_1 + m_2)}{c^5 \xi^4 (1 - e^2)^{5/2}} \left(1 + \frac{121}{304} e^2 \right). \tag{7}$$

In the last equations, ξ is the semimajor axis, e the eccentricity, t the time, m_1 and m_2 the mass of the first and second star in the binary, G is the gravitational constant and c the speed of light. In the case of a circular binary, as shown in Peters (1964), one can solve the differential equation for a binary with companion masses m_1, m_2 and initial semimajor axis ξ_0:

$$\xi(t) = (\xi_0^4 - 4\beta t)^{1/4}, \tag{8}$$

where

$$\beta = \frac{64}{5} \frac{G^3 m_1 m_2 (m_1 + m_2)}{c^5}. \tag{9}$$

This yields a decay time of $T_c(\xi_0) = \xi_0^4/(4\beta)$.

In the general case of eccentric binaries, one can integrate equation (7) numerically and compare the time evolution with the results of our simulations. Since Peters' formula is only valid for the leading order of gravitational radiation, we 'switch off' the terms 1 PN, 2 PN, 3 PN and 3.5 PN and only apply the 2.5 PN correction. In Figs 1 and 2, we show the time evolution of eccentricity and semimajor axis for a system with two BHs of masses $m_1 = 10 \, M_\odot$ and $m_2 = 1 \, M_\odot$. They agree very well up to the limit of validity of the PN expansion.

The 2.5 term only takes into account energy and angular momentum loss due to GWs. The 1 and 2 PN terms are conservative, they conserve energy and angular momentum, and they are the main contribution to periapsis shift.

In Figs 3 and 4, we show the time evolution for a binary in which we have taken into account the correcting terms 1 PN, 2 PN and 2.5 PN. Even though the 1 and 2 PN terms are conserving energy, the binary coalesces quicker than in the Peters approximation, because they change the orbital velocity and thus the 2.5 PN term acts slightly stronger. The small rise in eccentricity very close to the merger is a known effect of the PN expansion at the limits of its region of validity.
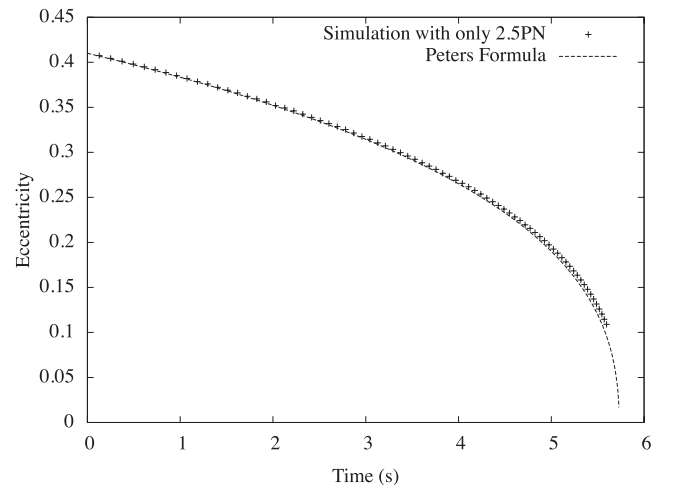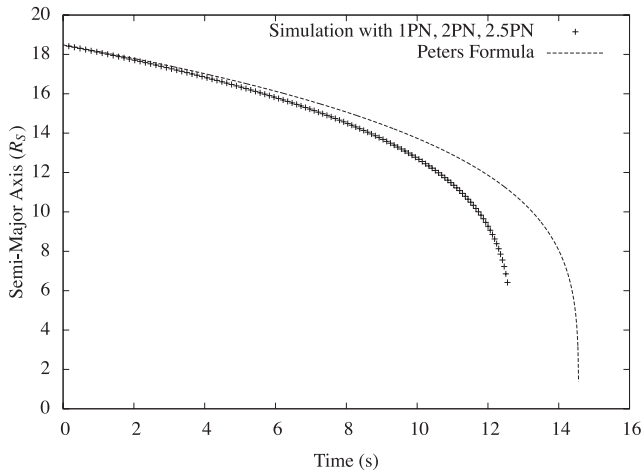

Figure 1. Comparison of the eccentricity evolution of the two-body integration and Peters' approximation.
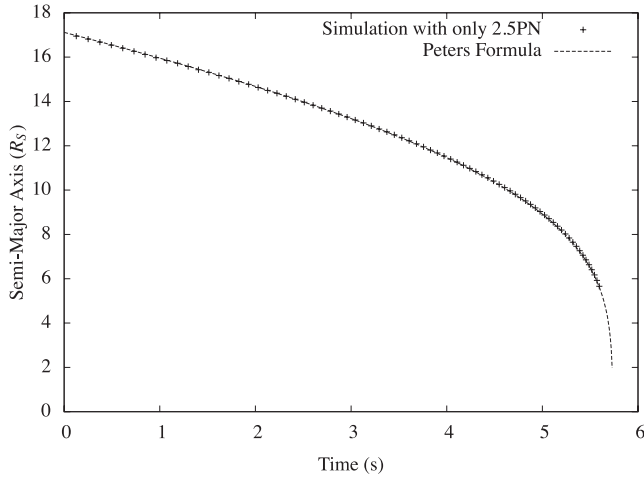
Figure 2. Comparison of the semimajor axis evolution of the two-body integration and Peters' approximation.
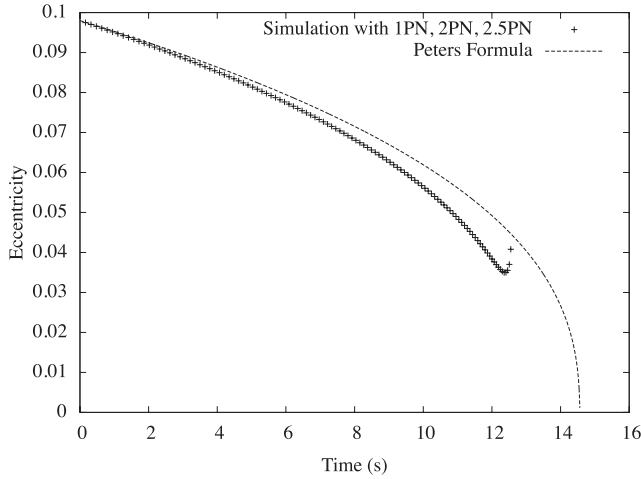
Figure 3. Comparison of the eccentricity evolution of the two-body integration with 1 PN, 2 PN and 2.5 PN terms and Peters' approximation.

Figure 4. Comparison of the semimajor axis evolution of the two-body integration with 1 PN, 2 PN and 2.5 PN terms and Peters' approximation.

The contribution at 3 PN and 3.5 PN order are small compared to the leading order, but these terms cause the orbit to diverge when the binary enters the last few $R_{\rm S}$.[3] This is an important effect, since with PN terms up to order 2.5 one could in principle let the system evolve until an overlap of the Schwarzschild radii. When including 3 PN and 3.5 PN, on the other hand, this becomes impossible and in order to avoid unphysical, divergent behaviour one has to abort the integration at larger separations. For this reason, we choose the criterion $r = 5R_{\rm S}$ where r is the instantaneous separation and $R_{\rm S}$ is the combined Schwarzschild radius.

3.2 Spinning binaries

3.2.1 Precession of angular momenta

In PN theory, the Newtonian angular momentum $\boldsymbol{L}_N = \boldsymbol{x} \times \boldsymbol{p}$, with $\boldsymbol{p} = r \times m \boldsymbol{v}$, is no longer conserved. In the case of non-spinning bodies, the direction of $\boldsymbol{L}_N$ is conserved and only the modulus $L_{\rm N}$ is gradually radiated away during inspiral. However, in the case of spinning bodies this no longer holds (Kidder 1995). Nonetheless, as in electromagnetic theory, both the total spin vector $\boldsymbol{S}$ and the angular momentum vector $\boldsymbol{L}$ precess around the total angular momentum vector $\boldsymbol{J} = \boldsymbol{L} + \boldsymbol{S}$. The angular momentum vector we use differs from the usual Newtonian definition:

$$\boldsymbol{L} = \boldsymbol{L}_N + \boldsymbol{L}_{\rm 1PN} + \boldsymbol{L}_{\rm SO} + \boldsymbol{L}_{\rm 2PN}. \tag{10}$$

With this definition, $\dot{\boldsymbol{J}} = 0$ up to 2 PN order. The 2.5 PN order, however, introduces radiation loss. Kidder (1995) estimated the precession frequency to the lowest order, i.e. $\boldsymbol{L} = \boldsymbol{L}_{\rm N}$. In the case of a single spinning body with mass $m_{\rm s}$ in a system with total mass m, the precession frequency of both $\boldsymbol{S}$ and $\boldsymbol{L}_{\rm N}$ is given by

$$\omega_{\rm p} = \frac{G|\boldsymbol{J}|}{2c^2r^3} \left(1 + 3\frac{m}{m_{\rm s}} \right). \tag{11}$$

As an example, let us consider a system of a maximally spinning black hole of mass $m_{\rm s} = 10\,{\rm M}_\odot$ and a non-spinning companion of mass $m_2 = 1\,{\rm M}_\odot$. We set the system on a circular orbit in the x–y plane with radius 10^8 cm with the initial spin of $m_{\rm s}$ in x-direction. This gives a total initial angular momentum of

$$|\boldsymbol{J}| = \sqrt{L_z(t=0)^2 + S_{1,x}(t=0)^2} = 1.12 \times 10^{44} \frac{\rm kg\,m^2}{\rm s}, \tag{12}$$

and thus a precession frequency of $\omega_{\rm p} = 0.18$ Hz. We use non-spinning PN terms up to 3.5 PN order and spin–orbit coupling up to next-to-leading order.

From Fig. 5, we can see that the approximate value for the period of the first precession cycle is (40.4 ± 0.4) s. This gives a value of $\omega_{\rm p,sim} = 0.15$ Hz. The small difference comes from the fact that the calculation assumes the approximation $\boldsymbol{L} = \boldsymbol{L}_{\rm N}$, and we are already in a very relativistic regime.

Even under the presence of spin–orbit precession, the direction of $\boldsymbol{J}_{\rm N}$ should be conserved. Fig. (6) shows the x–y projection of $\boldsymbol{J}_{\rm N}$ and $\boldsymbol{L}_{\rm N}$ during an inspiral. One can see that the direction of $\boldsymbol{J}_{\rm N}$ is approximately constant but that the modulus shrinks due to gravitational radiation. During this process, $\boldsymbol{L}_{\rm N}$ precesses about this direction. One can also see the wobbles in the precession of the orbital plane given by $\boldsymbol{L}_{\rm N}$, as described in the appendix of Kidder (1995). This is due to the fact that in reality the corrected $\boldsymbol{L}$ from equation (10) does the strict precession, which is not true for the

---

[3] Private communication with Seppo Mikkola and Cliff Will.
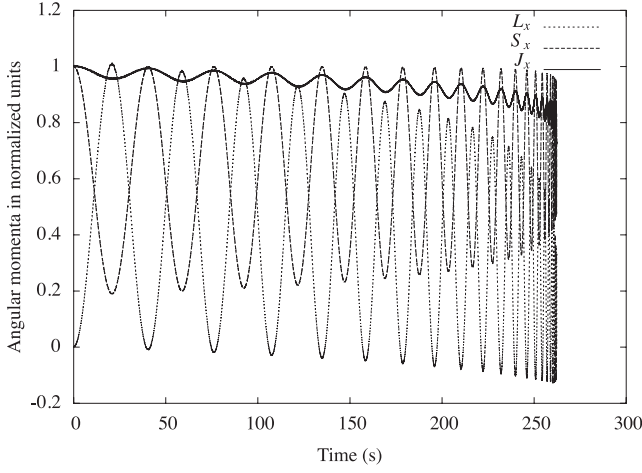
Figure 5. Angular momentum precession in the case of one spinning body. The total Newtonian angular momentum vector $\boldsymbol{J}_\mathrm{N}$ is approximately conserved.
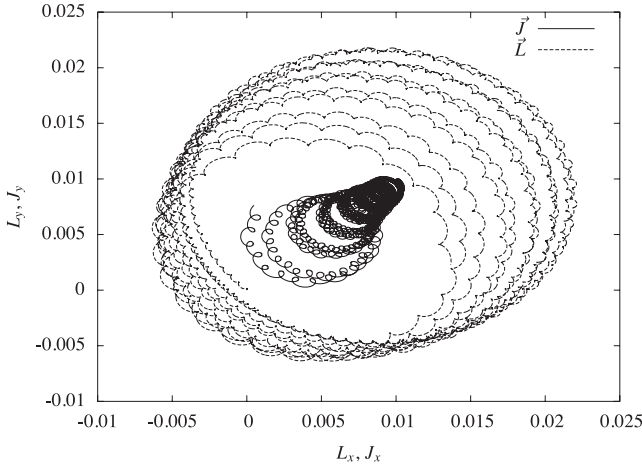
Figure 6. *X–Y* projection of the angular momentum precession in the case of two maximally spinning bodies. Both $\boldsymbol{J}_\mathrm{N}$ and $\boldsymbol{L}_\mathrm{N}$ are gradually radiated away as $\boldsymbol{L}_\mathrm{N}$ precesses about $\boldsymbol{J}_\mathrm{N}$.

Newtonian value $\boldsymbol{L}_\mathrm{N}$, and hence leads $\boldsymbol{L}_\mathrm{N}$ to wobble about the conserved $\boldsymbol{L}$.

The check of $\boldsymbol{J}$ conservation is a powerful way of testing the consistency of the approach to estimate the spin and angular momentum in the code.

3.3 Final spin approximation

In our code, we are subject to the limitations of our PN approach, which is not valid anymore when the relative speed becomes larger and larger, i.e. a few Schwarzschild radii before the merger. For this, we adopt the fitting formula of Rezzolla et al. (2008), derived from numerical simulations that address in full general relativity the last orbits of the binary, including merger and ringdown. We hence implement in the code the following formula for the modulus of the final spin (Rezzolla et al. 2008)

$$|\boldsymbol{a}_\mathrm{fin}| = \frac{1}{(1+q)^2}\Big[|\boldsymbol{a}_1|^2 + |\boldsymbol{a}_2|^2 q^4 + 2|\boldsymbol{a}_2||\boldsymbol{a}_1|q^2 cos\,\alpha$$

$$+2(|\boldsymbol{a}_1|cos\,\beta + |\boldsymbol{a}_2|q^2 cos\,\gamma)|\boldsymbol{l}|q + |\boldsymbol{l}|^2 q^2\Big]^{1/2}, \quad (13)$$
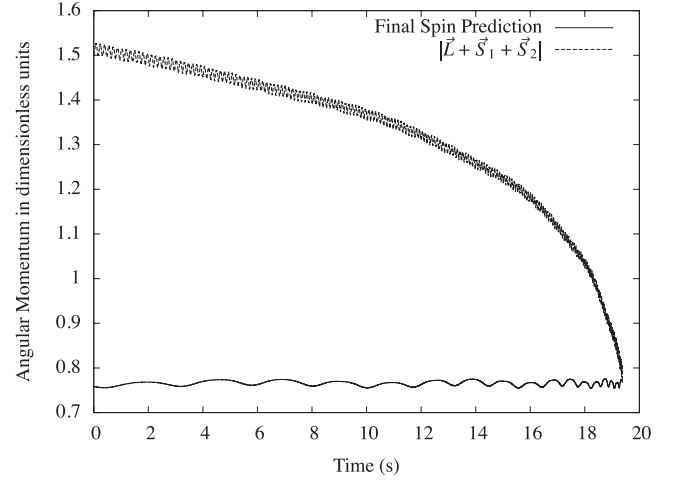
Figure 7. Comparison between the current final spin prediction and the actual total angular momentum of the binary system.

where $q = m_2/m_1$ is the mass ratio, $\boldsymbol{a}_1$ and $\boldsymbol{a}_2$ the dimensionless spin vectors and the angles are defined as

$$cos\,\alpha = \hat{a}_1 \cdot \hat{a}_2,$$

$$cos\,\beta = \hat{a}_1 \cdot \hat{l},$$

$$cos\,\gamma = \hat{a}_2 \cdot \hat{l}. \quad (14)$$

Therefore, so as to derive a value for the spin after merger, we need the individual spin vectors $\boldsymbol{a}_1$, $\boldsymbol{a}_2$ and the orbital angular momentum (OAM) at an arbitrary point in time during inspiral. $\boldsymbol{l}$ is a function of the OAM, given by

$$|\boldsymbol{l}| = \frac{s_4}{(1+q^2)^2}(|\boldsymbol{a}_1|^2 + |\boldsymbol{a}_2|^2 q^4 + 2|\boldsymbol{a}_1||\boldsymbol{a}_2|q^2 cos\,\alpha)$$

$$+\left(\frac{s_5\eta + t_0 + 2}{1+q^2}\right)(|\boldsymbol{a}_1|\,cos\,\beta + |\boldsymbol{a}_2|q^2\,cos\,\gamma)$$

$$+2\sqrt{3} + t_2\eta + t_3\eta^2, \quad (15)$$

where we use the fitting factors s_i, t_i given in Rezzolla et al. (2008). With equation (13) to (15) in hand, one can check whether in the regime in which PN is valid, the simulation is consistent with this formula, in the sense that

(i) the total angular momentum must converge to the predicted absolute value,

(ii) the predicted final value should be independent of the time until coalescence.

Fig. 7 shows the time evolution of both the predicted absolute value of the final spin at any given time during the inspiral and the actual total angular momentum. As one can see, for equal masses this gives a consistent value. $\boldsymbol{J}$ is decreasing due to gravitational radiation until it reaches the prediction. At the latest times close to the merger, there will remain a small difference between $\boldsymbol{J}$ and the predicted value due to the cut-off at $5R_\mathrm{S}$ and due to other effects that are part of the numerical relativity simulations but not modelled in our PN integration.

3.4 Energy conservation

Since NBODY6 is a code to integrate Newtonian systems, it regularly checks whether the total energy of the system is conserved within

some tolerance for numerical errors. In this work, we have added relativistic terms in the PN approximation, so that this is no longer the case: (i) the dissipation, mainly by the 2.5 PN term, causes a cumulative energy loss that has to be tracked and subtracted from the total energy. On the other hand, (ii) even the non-dissipative terms cause oscillations in the Newtonian energy, since only the modified expression,

$$E = E_{\text{Newt}} + E_{2.5\text{PN,dis}} + E_{1\text{PN}} + E_{2\text{PN}} + E_{3\text{PN}} + \cdots \qquad (16)$$

is conserved at any given time. We thus calculate and subtract the corrections up to 3 PN order from the total energy in order to construct the conserved quantity E. In this way, we are able to verify energy conservation in the same way as it is usually done in purely Newtonian codes. This works well if the relativistic corrections are small. However, when $g_{\text{PN}}/g \approx 1$ the error induced by PN corrections will dominate and it becomes impossible to verify the correct integration of the system. In order to avoid this, one could decide an even larger distance threshold for merging two bodies into one or a criterion based on the relative strength of the PN corrections.

4 STELLAR-MASS BINARY MERGERS IN A CLUSTER: SOURCES OF GWS FOR GROUND-BASED DETECTORS

It is well-established that most galaxies should harbour a massive black hole in their centre, with a mass of some $10^{6-9}\,\mathrm{M_\odot}$ (see e.g. Ferrarese et al. 2001; Kormendy & Gebhardt 2001; Ferrarese & Ford 2005). The densities observed may even exceed the core density of globular clusters by a factor of 100, and hence achieve about 10^7–$10^8\,\mathrm{M_\odot\,pc^{-3}}$. Mass segregation creates a flow of compact objects towards the centre of the system (Lee 1987; Miralda-Escudé & Gould 2000; Khalisi, Amaro-Seoane & Spurzem 2007; Preto & Amaro-Seoane 2010; Amaro-Seoane & Preto 2011) and may build up a cluster which could reproduce the effect of a massive black hole (MBH). Indeed, this has been used as an alternative to explain phenomena related to cluster evolution, like G1 and M15 (Gebhardt, Rich & Ho 2002; van der Marel et al. 2002; Baumgardt et al. 2003a,b; Banerjee & Kroupa 2011). Nonetheless, for a globular cluster, compact objects such as stellar black holes are very likely expulsed via three-body interactions (Phinney & Sigurdsson 1991; Kulkarni, Hut & McMillan 1993; Sigurdsson & Hernquist 1993; Portegies Zwart & McMillan 2000). Lee (1995) proved that for $\sigma \gtrsim 300\,\mathrm{km\,s^{-1}}$, the merger induced by gravity loss in clusters with two components is shorter than the required time-scale for a third star to interact with a binary, so that clusters with higher velocity dispersions will not run into that problem. In this section, we will test the robustness of our code by running simulations of dense stellar clusters with a very high velocity dispersion to trigger a large number of relativistic coalescences.

4.1 Initial conditions

To run a stress test on our implementation, we will consider that the clusters are represented by an isotropic Plummer sphere containing $N = 1000$ stellar remnants of equal mass m. We use N-body units and choose a scaling according to KAS06 to trigger a significant amount of relativistic mergers to test the code. We set the central velocity dispersion to $\sigma_{\text{cen}} \approx 4300\,\mathrm{km\,s^{-1}}$, which is equivalent to fixing the ratio

$$\frac{\sigma_{\text{cen}}}{c} = \frac{1}{70}. \qquad (17)$$
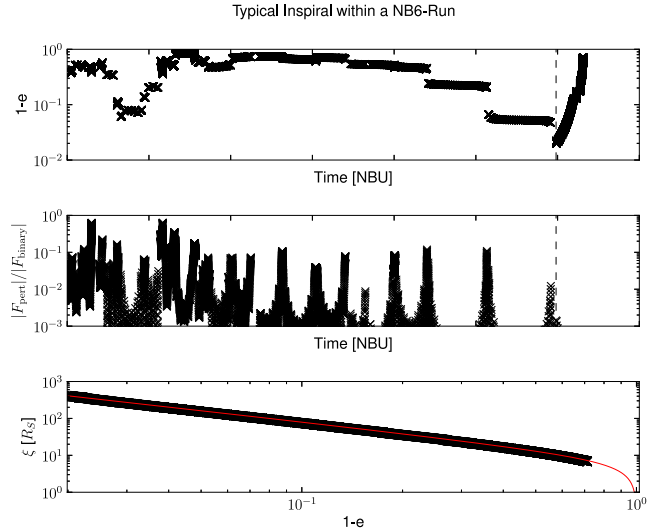
Figure 8. Top panel: eccentricity evolution of one dynamically formed binary. First it is driven by Newtonian perturbations until the eccentricity reaches a critical value, from which the rapid circularization sets in. The dashed line marks the point from which we integrated equation (7) shown in the bottom panel. Middle panel: perturbing force relative to the binary force. Strong changes in eccentricity are caused by strong Newtonian perturbations. Bottom panel: inspiral as recorded in the simulation, compared to the analytical solution of equation (7) as the solid line.

In other words, the speed of light 'in code units' is $c = 70$. We consider therefore a cluster of compact objects with the same mass, spinning with a dimensionless spin parameter a and we consider three different initial spin setups for the compact objects at the time $T = 0$.

  (i) Non-spinning ($a = 0$).
  (ii) Maximally spinning in the z-direction ($a = 1$).
  (iii) Random magnitude and orientation.

## 4.2 Demonstration of a typical binary merger

We demonstrate here the evolution of a relativistic binary that has been formed dynamically within one of the non-spinning setups. Since we want to compare the decay to the approximation given by equation (7), only the dissipative 2.5 PN term has been included. Fig. 8 shows the evolution of the orbital elements and the Newtonian perturbation by third bodies relative to the binary force. The eccentricity evolves due to Newtonian perturbation until it reaches a critical value and the GW-driven inspiral sets in. From this point, the solution of equation (7) is plotted for comparison. We note that in all plotted data points, the PN terms have been switched on and we thus confirm the robustness of our implementation under the presence of strong Newtonian perturbations.

4.3 Runaway growth

Because our system consists of very relativistic objects, almost any binary that forms and is regularized will undergo a quick merger due to the loss of orbital energy and due to the dissipative 2.5 PN term. Around the time of the core collapse, i.e. after some $\sim 15\,T_{\text{rlx}}(T=0)$, with $T_{\text{rlx}}(T=0)$ the initial relaxation time of the cluster, a series of mergers leads to the formation of one particular BH in the system that rapidly grows in mass and becomes much more massive than the other objects. Therefore, we say that the object runs away in
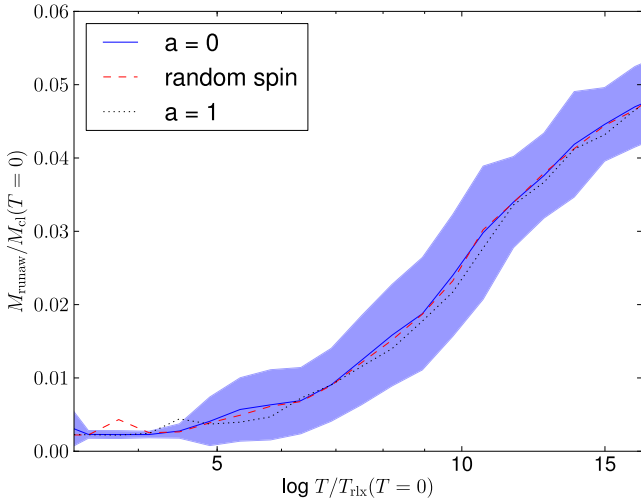
Figure 9. Mass of the runaway body, M_{runaw}, for each setup, averaged over 500 runs. $M_{\mathrm{cl}}(T = 0)$ is the total mass of the cluster at the time $T = 0$ and $T_{\mathrm{rlx}}(T = 0)$ the initial relaxation time of the cluster. The shaded area shows the standard deviation for the $a = 0$ case.
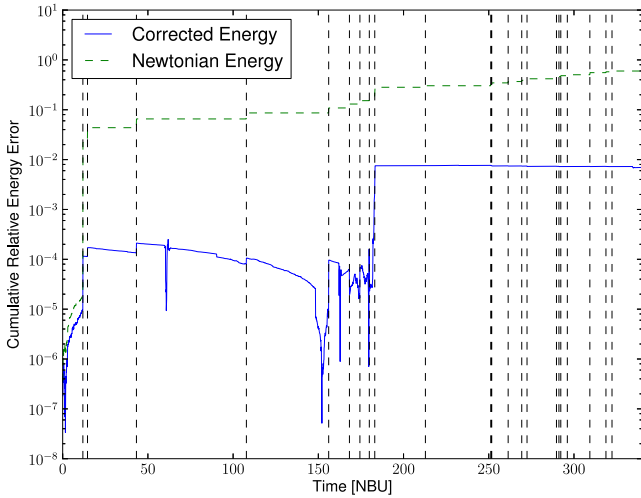
Figure 10. Cumulative relative energy error in a typical simulation. In this case, we have 22 mergers, indicated by the dashed vertical lines, which cause the Newtonian energy error to grow significantly. Our alternative method to check for energy conservation leads to smaller fluctuations.

mass. This is a consequence of the increase in cross-section for GW capture. The time evolution of the mass of this runaway object is shown in Fig. 9. As we can see, after some $\sim 15\,T_{\mathrm{rlx}}(T = 0)$, the runaway object has achieved ~ 5 per cent $M_{\mathrm{cl}}(T = 0)$, a value similar to the case studied in KAS06, their fig. 1 around 450 time units.

An important issue that we need to address is the energy conservation in the simulations. In Fig. 10, we show both the usual Newtonian energy and the corrected value, computed with equation (16) for a simulation with the same configuration as before but with $N = 2000$ bodies. The Newtonian energy error grows with every single merger due to the dissipative PN terms. The corrected value for the energy conservation in our approach fluctuates significantly less and stays below 1 per cent. The absolute value of the error depends on the nature of the merger. Head-on collisions dissipate the lowest amount of energy, while gradual inspirals lose the maximum amount before merger. The significant jump at $T = 183$ corresponds to a binary which has spent a very long inspiral time due to a low
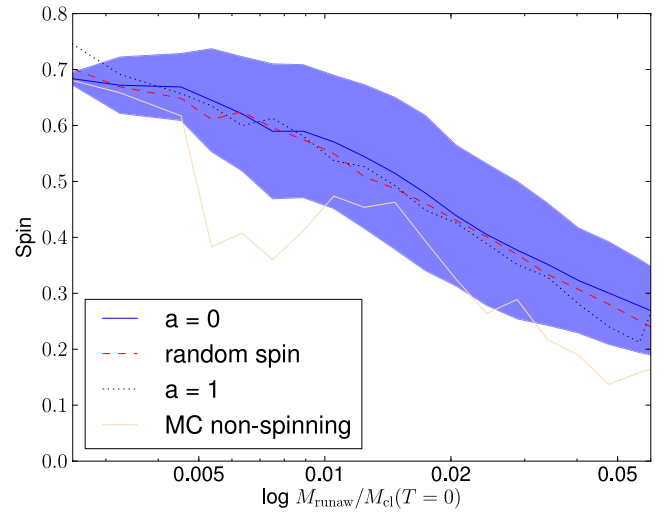
Figure 11. Spin of the runaway body in each simulation, averaged over 500 runs. The shaded area shows the standard deviation for the $a = 0$ case. All initial spin setups lead to a similar evolution, except for the very first data point which is slightly higher for the maximally spinning initial conditions.

eccentricity and a high initial separation. This causes rather high errors in the numerical integration of the dissipated energy at 2.5 PN order and thus contributes most to the total error, while some of the other mergers only cause relative errors of $\approx 10^{-4}$.

The absolute energy error depends crucially on the cut-off radius at which we end the integration and merge two bodies into one, because this sets the highest velocity we have to deal with in the binary. In this run, we chose $10R_{\mathrm{S}}$. For smaller values, even the corrected error grows to the order of the total energy of the system. We note that even with larger errors induced by the dissipative PN terms, the global behaviour of the simulation is not affected by the particular choice of the merger radius. If one wants a powerful energy conservation check it is reasonable to choose larger cut-off radii.

In order to be able to make a statistical comparison between each of the three spin setups and the potential impact on the evolution of the runaway body, we perform 500 simulations for each initial spin setup and show the mass averaged over each time bin. We can see in Fig. 11 the evolution of the spin for all three cases against the accumulated mass of the runaway object. Its formation is approximately the same in all three different scenarios, and consistent with the results of KAS06. Nonetheless, the precise point in time where the onset of the runaway process takes places depends sensitively on the scaling. In any case, the choice for the initial distribution of spins is washed out and all three cases show a consistent evolution for the runaway body. We additionally perform 500 Monte Carlo realizations of the scenario where one object merges with non-spinning compact objects coming in at random angles using the same final spin prediction as in the N-body code, so that we can test the statistical study. We depict the Monte Carlo spin evolution in Fig. 11 and confirm that this evolution is consistent with our N-body analysis within some scattering.

4.4 Evolution of individual spins

We now focus on the compact objects that have experienced only a few mergers. While the evolution of the spin of the runaway object quickly washes out any information regarding the initial spins, in the case of the other compact objects that do not undergo so many
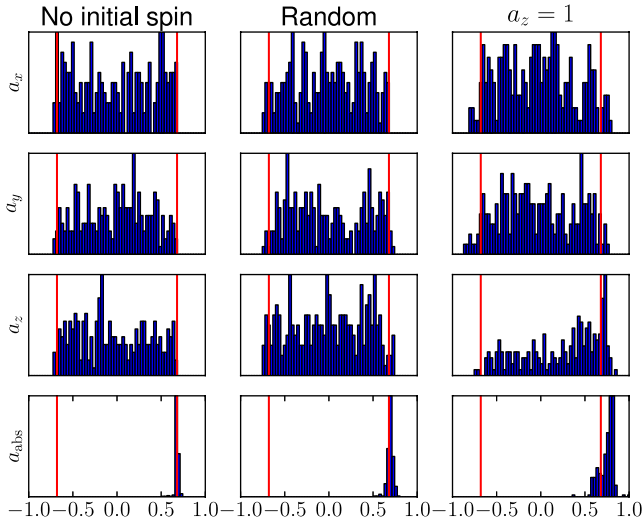
Figure 12. Spin distribution for those objects that have undergone at least one merger during the whole evolution of the cluster but not more than four. In the top panels, we show three different initial choices for the spin of the BHs. From the left to the right, we have first a cluster in which initially the BHs do not have spin, then a random value and in the last column a maximally spinning configuration around the *z*-direction. From the top to the bottom panels, we display the *x*-, *y*-, *z*- and absolute component of the spin ranging between −1 and 1 (a_x, a_y, a_z, a_{abs} shown on the left *y*-axis of the panels, respectively). The red lines depict the values −0.68 and +0.68.

mergers, there is a dependence on the initial configuration even after core collapse. This is particularly interesting, since a trend in the evolution of the spin measurable with the advanced detectors would provide us with valuable information about the spin evolution of compact objects in clusters.

As mentioned in Section 2.3, we did not include BH recoil. For any BH merger involving significantly spinning BHs, the recoil velocity can exceed the escape velocity and these merger products could thus leave the cluster. This means that the distribution presented here contains BHs that might no longer be part of the cluster itself.

In Fig. 12, we show the end distribution of spins for different initial configurations of the spin distribution for an otherwise identical system.

The configuration which initially had no spins is useful for comparison with the other systems. While the *x*-, *y*- and *z*-components individually show no clear trend, the absolute value is $a_{abs} = (0.69 \pm 0.02)$. If we move on to the second configuration, in which we initially assign all compact objects a spin but of random value, the final distribution is scattered around the same value, displayed with a red line in each of the panels at 0.68. In this case, the final value and standard deviation are $a_{abs} = 0.71 \pm 0.03$. Finally, if we give all compact objects initially a maximum value and set them in a preferred direction, which we arbitrarily choose to be the positive *z*-direction, the final distribution has a value of $a_{abs} = 0.76 \pm 0.08$.

In Fig. 13, we can also see this dependence. In the plot, we display the time evolution of the total spin angular momentum in the cluster, including the runaway object which carries most of the spin angular momentum. In the case of an initially non-spinning configuration, the spin builds up from OAM and converges to a generic value in a similar way to what we showed in Fig. 12. We are limited in our analysis to derive the exact value to which the curve converges because of an accumulation of numerical errors.
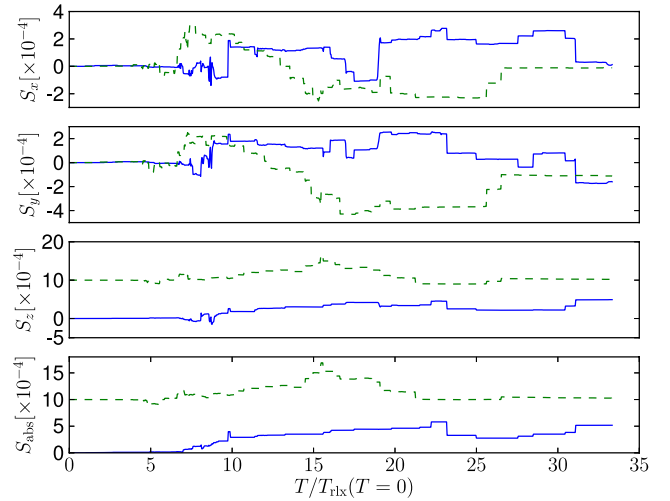
Figure 13. Dashed green: total spin angular momentum for a cluster in which the remnants are initially maximally spinning in the *z*-direction. Solid blue: total spin angular momentum for an initially non-spinning configuration.

5 CONCLUSIONS

In this work, we have presented the first implementation of the effect of the spin for the treatment of relativistic mergers in a direct-summation *N*-body integrator. For that, we modify the calculation of the gravitational forces among particles using PN up to 3.5 PN order and the spin–orbit coupling up to next-to-lowest order and the lowest order spin–spin coupling.

We then check our implementations by running a series of tests to compare with results based on analytical derivations, for isolated two-body binaries and confirm the robustness of our approach. We also present a way to check for the correct integration of a system of *N* particles based on tracking the total energy, a usual test with this kind of integrators. Our method is valid provided the number of relativistic mergers in the system is low.

The final acid test of the implementation is to compare the global dynamical behaviour of a relatively large number of BHs with the new relativistic behaviour for binaries with well-known results based on similar approaches. More specifically, we run a similar test to that of KAS06 and obtain very similar results, which confirms the correct incorporation of the new terms in the code, since the initial spin distribution does not significantly change the global evolution of the system. This is so, because if two non-spinning, equal mass compact objects merge, the merger product will be spinning with $a \approx 0.68$ (Damour & Nagar 2007) in the direction of the angular momentum. Since in a Plummer sphere there is no preferred direction in the distribution of the two-body angular momenta, this leads to a randomization of the non-spinning distribution quickly. In the scenario of two maximum spins in the *z*-direction, i.e. individual spins of $S = Gm^2/c$ with equal masses *m*, the approximate angular momentum in the last stable orbit before merger is of the same order and thus also rotate the spins and similarly wash out the initially preferred direction.

For the larger subset of BHs that undergo a lower number of coalescences, which is more interesting since it is closer to what one could expect to see in a realistic cluster, we find that the evolution of the spin for consecutive mergers has a trend that oscillates around the value predicted by Damour & Nagar (2007), but with a scatter that is a fingerprint of the initial distribution of the isolated BHs, before they merged with any other in the system. This is particularly

interesting, since this trend is what will determine the value of the spin that one can expect to see in globular clusters, and should be carefully assessed when developing the waveform banks to do the data analysis for the first detection.

Although, the systems that we have explored in this work cannot be envisaged as representative examples of the grounds for which we expect the advanced detectors to observe relativistic mergers, the initial study of the behaviour of the code is a requirement before we proceed to more realistic systems, and has provided us with initial results which could play a crucial role in detection.

In particular, an immediate goal of our next research will be the study of the spin distribution and evolution in a dense stellar cluster with a realistic number of stars and including stellar evolution and primordial binaries, such as in Downing et al. (2010, 2011), but with a more accurate direct *N*-body integrator. The history and distribution of black holes in a dense star cluster is also important for observing them in the electromagnetic windows, since it determines e.g. number and distribution of X-ray binaries and encounters between black holes and other compact objects such as neutron stars or white dwarfs.

Giersz et al. (2013) clearly show in their (non-relativistic) star cluster simulations using the Monte Carlo code that quite a few BHs and BH–BH binaries are formed and play a role for the dynamics of the central region. The presence of BHs may explain the size differences between red and blue globular clusters (Downing 2012) and affect the number of blue stragglers in a cluster (Hypki & Giersz 2013). These papers also discuss that relativistic recoils after merger are not only important for the GW signal itself, but it is an important ingredient for correct modelling of globular clusters.

The kind of analysis we have presented in this work will soon have interesting applications, taking into account that the advanced ground-based detectors LIGO and VIRGO will have achieved their design sensitivity as soon as 2016–2017.

REFERENCES

Aarseth S. J., 1963, MNRAS, 126, 223
Aarseth S. J., 2003, Gravitational N-Body Simulations. Cambridge Univ. Press, Cambridge (ISBN 0521432723)
Aarseth S. J., 2012, MNRAS, 422, 841
Ahmad A., Cohen L., 1973, J. Comput. Phys., 12, 389
Ajith P. et al., 2007, Class. Quantum Gravity, 24, 689
Ajith P. et al., 2009, Phys. Rev. D, 79, 129901
Amaro-Seoane P., Preto M., 2011, Class. Quantum Gravity, 28, 094017
Banerjee S., Kroupa P., 2011, ApJ, 741, L12
Banerjee S., Baumgardt H., Kroupa P., 2010, MNRAS, 402, 371
Baumgardt H., Hut P., Makino J., McMillan S., Portegies Zwart S., 2003a, ApJ, 582, L21
Baumgardt H., Makino J., Hut P., McMillan S., Portegies Zwart S., 2003b, ApJ, 589, L25
Benacquista M. J., Downing J. M. B., 2011, preprint (arXiv:1110.4423)
Blanchet L., Iyer B. R., 2003, Class. Quantum Gravity, 20, 755
Buonanno A., Damour T., 1999, Phys. Rev. D, 59, 084006
Buonanno A., Chen Y., Vallisneri M., 2003, Phys. Rev. D, 67, 104025
Buonanno A., Pan Y., Pfeiffer H. P., Scheel M. A., Buchman L. T., Kidder L. E., 2009, Phys. Rev. D, 79, 124028
Damour T., Nagar A., 2007, Phys. Rev. D, 76, 044003
Downing J. M. B., 2012, MNRAS, 425, 2234
Downing J. M. B., Benacquista M. J., Giersz M., Spurzem R., 2010, MNRAS, 407, 1946
Downing J. M. B., Benacquista M. J., Giersz M., Spurzem R., 2011, MNRAS, 416, 133
Faye G., Blanchet L., Buonanno A., 2006, Phys. Rev. D, 74, 104033
Ferrarese L., Ford H., 2005, Space Sci. Rev., 116, 523
Ferrarese L., Pogge R. W., Peterson B. M., Merritt D., Wandel A., Joseph C. L., 2001, ApJ, 555, L79
Gebhardt K., Rich R. M., Ho L. C., 2002, ApJ, 578, L41
Giersz M., Heggie D. C., Hurley J. R., Hypki A., 2013, MNRAS, 431, 2184
Hypki A., Giersz M., 2013, MNRAS, 429, 1221
Khalisi E., Amaro-Seoane P., Spurzem R., 2007, MNRAS, 374, 703
Kidder L. E., 1995, Phys. Rev. D, 52, 821
Kormendy J., Gebhardt K., 2001, in Wheeler J. C., Martel H., eds, AIP Conf. Ser. Vol. 586, 20th Texas Symposium on Relativistic Astrophysics. Am. Inst. Phys., New York, p. 363
Kulkarni S. R., Hut P., McMillan S., 1993, Nat, 364, 421
Kupi G., Amaro-Seoane P., Spurzem R., 2006, MNRAS, 371, L45 (KAS06)
Kustaanheimo P. E., Stiefel E. L., 1965, J. Reine Angew. Math., 218, 204
Lee H. M., 1987, ApJ, 319, 801
Lee H. M., 1995, MNRAS, 272, 605
Lousto C. O., Campanelli M., Zlochower Y., Nakano H., 2010, Class. Quantum Gravity, 27, 114006
Miller M. C., Lauburg V. M., 2009, ApJ, 692, 917
Miralda-Escudé J., Gould A., 2000, ApJ, 545, 847
Peters P. C., 1964, Phys. Rev., 136, 1224
Phinney E. S., Sigurdsson S., 1991, Nat, 349, 220
Pollney D. et al., 2007, Phys. Rev. D, 76, 124002
Portegies Zwart S. F., McMillan S. L. W., 2000, ApJ, 528, L17
Preto M., Amaro-Seoane P., 2010, ApJ, 708, L42
Rezzolla L., Barausse E., Dorband E. N., Pollney D., Reisswig C., Seiler J., Husa S., 2008, Phys. Rev. D, 78, 044002
Santamaría L. et al., 2010, Phys. Rev. D, 82, 064016
Sigurdsson S., Hernquist L., 1993, Nat, 364, 423
Tagoshi H., Ohashi A., Owen B. J., 2001, Phys. Rev. D, 63, 044006
van der Marel R. P., Gerssen J., Guhathakurta P., Peterson R. C., Gebhardt K., 2002, AJ, 124, 3255
von Hoerner S., 1960, Z. Astrophys., 50, 184
von Hoerner S., 1963, Z. Astrophys., 57, 47
Yunes N., Berti E., 2008, Phys. Rev. D, 77, 124006

This paper has been typeset from a TEX/LATEX file prepared by the author.